Scientific Research Publishing

Engineering, 2022, 14, 185-216
https://www.scirp.org/journal/eng
ISSN Online: 1947-394X
ISSN Print: 1947-3931

The Solving of the Inverse Thermal Conductivity Problem for Study the Short Linear Heat Pipes

Arkady Vladimirovich Seryakov

LLC "Rudetransservice", Veliky Novgorod, Russia
Email: seryakovav@yandex.ru

How to cite this paper: Seryakov, A.V. (2022) The Solving of the Inverse Thermal Conductivity Problem for Study the Short Linear Heat Pipes. *Engineering*, **14**, 185-216.
https://doi.org/10.4236/eng.2022.146018

Received: April 11, 2022
Accepted: June 27, 2022
Published: June 30, 2022

Abstract

The results of studies by solving the inverse thermal conductivity problem of the heat capacity of evaporator of the short linear heat pipes (HP's) with a Laval nozzle-liked vapour channel and intended for cooling spacecraft and satellites with strict take-off mass regulation are presented. Mathematical formulation of the inverse problem for the HP's thermal conductivity in one-dimensional coordinate system is accompanied by the measurement results using the monotonic heating method in a vacuum adiabatic calorimeter the HP's surface temperatures along the longitudinal axis over the entire temperature load range, thermal resistance, and arrays of thermal power data on the evaporator Q_{ev} and vortex flow calorimeter Q_{cond} for the condensation surface allow us to estimate the average value of the evaporator heat capacity C_{ev} by solving the inverse thermal conductivity problem in the HP's evaporator region. Since at the beginning of working fluid boiling for a certain time interval, the temperature of the capillary-porous evaporator remains close to constant, and with the continuation of heating and by solving the inverse thermal conductivity problem, it becomes possible to calculate the heat capacity of the working evaporator and the evaporation specific heat of the boiling working fluid and compare it with the table values.

Keywords

Short Linear HP's, The Inverse Problem of Thermal Conductivity,
The Monotonic Heating Method, Thermal Resistance and Heat Capacity

1. Introduction

The current development level of the computer technology and computing technologies allows us to significantly expand the class of applied problems to be

solved. Those scientific and technical problems of the HP's heat transfer that have traditionally been tried to be considered analytically are increasingly being analysed and solved with the help of numerical methods using specialized software for engineering calculations. We are talking about the application of computational programs for solving inverse problems of thermal conductivity of solids in one-dimensional formulation and the use of the obtained methods for analysing the operation of short HP's with a Laval nozzle-liked vapour channel and a large amount of working fluid in the capillary-porous insert and evaporator. Numerical methods have received the greatest application due to a number of specific advantages, the main of which is their relatively simple implementation on computers [1] [2] [3].

Inverse problems are characterized by instability of their solutions, which manifests itself in the occurrence of large numerical changes in the solution with small changes in the initial data.

Tasks of this type are called incorrectly assigned tasks or ill-posed problems [4] [5] [6] [7] [8]. A large section of ill-posed problems consists of inverse problems that arise in cases where the necessary initial and boundary data for the formulation of a direct correct problem, for example, the direct heat conduction problem, are not available, but there is some additional information about the solution that allows us to formulate the inverse problem. Such problems include inverse problems of thermal conductivity (IPTC) [9] [10] [11].

The general nonlinear problem of non-stationary HP's thermal conductivity can be considered as a set of three nonlinear problems: a problem in which the nonlinearity arises due to the temperature dependence of the coefficients of the main equation; a problem in which the boundary conditions are nonlinear, for example, due to evaporation or boiling of the working fluid in the evaporator; and a problem in which the nonlinearity arises due to the temperature dependence of internal heat sources (sinks). The boundaries between these problems are very conditional, since some transformations allow you to switch from one type of nonlinearity to another, which sometimes simplifies the use of certain methods for solving nonlinear problems.

The main difficulty in the approximate solution of ill-posed problems is the choice of regularization parameters to achieve the stability of the solution. To determine it, the following approaches are most widely used [12] [13] [14] [15]: the choice of the regularization parameter by the remainder in the different functional; the use of the variational method with the calculation of the Lagrange function (Lagrangian); an iterative method in which the regularization parameter is the number of iterations corresponding to the error of the input data [15]. This latter well-known methodology of solving inverse heat transfer problems is quite effective and is widely used in space technology, military science, aviation, but its implementation requires a large amount of computational work [12] [13].

When solving inverse problems for equations of mathematical physics, gradient iterative methods are widely used in the variational formulation of the in-

verse problem [13]. In this paper, we consider the simplest gradient iterative method for approximate solution of the retrospective (with inverse time) inverse problem of the evaporator heat capacity of short HP's with a vapour channel similar to a Laval nozzle with a known value of thermal resistance R_{HP} or thermal conductivity coefficient λ_{HP}. In addition, in our inverse problem, the initial condition is iteratively refined, *i.e.*, at each iteration, the usual boundary value problem for the heat equation is solved.

In addition the heat source in the HP's evaporator depends only on the time τ, and the temperature field $T(z)$ in the entire geometric space of the HP inside the adiabatic calorimeter is experimentally determined using copper-constantan surface thermocouples. These measurements guarantee that the inverse problem has an unambiguous solution, but this solution is unstable; therefore, additional regularization and the use of the variational method [14] [15] with Lagrange multipliers to determine the optimal values of the parameters in the different functional are necessary to solve the problem. This method gives rapidly converging successive approximations of the exact solution.

A simple algorithm for the numerical solution of a one-dimensional inverse problem by the coefficient of thermal conductivity for calculating the heat capacity of a short HP's evaporator with a boiling working fluid has been developed and implemented in the FORTRAN system for a PC. In this case, an important factor is the temperature of the external surface of the capillary-porous HP's evaporator, which is close to a constant value. With further heating, the level of boiling working fluid in the HP's evaporator slowly decreases, and the temperature of the external surface also slowly decreases. And this allows us to calculate the extreme behavior of the evaporator heat capacity and estimate the specific heat of working fluid boiling in them.

In addition, our simple algorithm is convenient for its implementation in the measuring scheme of an adiabatic vacuum calorimeter for the study of short HP's. The capabilities of this algorithm are illustrated by solving several specific problems for calculating the heat capacity of short solids under monotonic heating at moderate temperatures, including a model problem with the evaporation of diethyl ether and, consequently, with variable initial conditions.

Thus, the main purpose of this work is to expand the research capabilities of HP heat pipes, solve inverse problems of thermal conductivity with their help and clarify the thermophysical characteristics of working fluids when boiling occurs in an HP capillary-porous evaporator. The proposed new application of the developed mathematical ideas makes it possible to significantly increase the scope of HP and raise the depth and vastness of the results obtained.

HP's Thermophysical Analysis

When analyzing short HP's, the thermophysical characteristics are represented by the so-called effective properties, and the process of heat transfer along the vertically oriented z coordinate is described by the thermal conductivity equa-

tion:

$$\rho_{HP} C_{eff}(T) L_{HP} F_{HP} \frac{\partial T}{\partial \tau} = \nabla\left(\lambda_{eff}(T) \nabla T\right). \quad (1)$$

The specific heat capacity of the HP's is determined additively by the formula (2) when the components and materials are characterized by the absence of chemical interaction between them.

$$\overline{C}_{HP}(T) = \sum\nolimits_j \psi_j C_j(T). \quad (2)$$

where ψ_j is the mass fractions of the HP's components, C_j is their heat capacity's. The effective thermal conductivity λ_{eff} as an additive sum thermophysical characteristics of the components can be presented only in simple cases, in particular for HP's in a non-working state.

During the phase transformation of the fluid component, for example, during the working fluid boiling process in the HP's evaporator, Equation (1) must be supplemented with an additional source function:

$$Y(T) = \rho_{HP} r_j(T) \frac{\partial \psi_j}{\partial \tau} = \rho_{HP} r_j(T) \frac{\partial \psi_j}{\partial T} \frac{\partial T}{\partial \tau}. \quad (3)$$

where $r_j(T)$ is the specific heat of the phase transformation of the j – th component.

Taking into account (2), Equation (1) can also be used in the presence of phase transformations in the HP with a new average heat capacity:

$$\overline{C}_{HP}(T) = C_{eff}(T) - r_{sp}(T).$$

The heat conduction equation in one-dimensional Cartesian coordinate system for calculating the heat propagation in a vertically oriented short linear HP's with a cylindrical body along the longitudinal z-axis, during monotonic heating in an adiabatic calorimeter without heat losses through the side walls is written as follows:

$$\begin{aligned} &\rho_{HP} C_v(T) L_{HP} F_{HP} \dot{T}(z,\tau) = L_{HP} F_{HP} \frac{1}{z} \frac{\partial}{\partial z} \frac{1}{R_{HP}(T)} \frac{\partial t(z,\tau)}{\partial z}; \\ &R_{HP}(T) = \frac{L_{HP}}{\lambda_{HP}(T) F_{HP}}. \end{aligned} \quad (4)$$

The process of heating and heat transfer using HP's is endothermic process, parameter $Y(T)$ has a negative value, $Y(T) \le 0$, which implies the principle of maximum and the uniqueness of the thermal conductivity equation solution [4] [5]. However, if the parameter $Y(T)$ is positive, $Y(T) > 0$ in general case it may turn out that the heat capacity $c_v(T)$ in some temperature range is negative, $c_v(T) < 0$, which may lead to instability of the numerical solution and incorrectness of the direct problem for Equation (4).

The measurement part of our method consists in a system for measuring the thermal power entering to the evaporator, the thermal power entering in the vortex flow calorimeter and the temperature distribution of the HP's surface inside the adiabatic calorimeter. In the case of using a vacuum adiabatic calorime-

ter with slow monotonous heating, the temperature distribution along the HP's body makes it possible to distinguish characteristic areas (zones) of the HP's, for example, the zone of the evaporator, the temperature in which, under a high temperature load, is close to constant for a fairly long boiling time (several tens of minutes), the time when the level of the working fluid in the capillary-porous evaporator decreases from the initial value h = 3.5 mm to the final value h = 0.02 – 0.01 mm and even less than this value.

The monotonic heating mode is extremely informative for the study of the short HP's with the phase transformation (boiling) of the working fluid in the evaporator [3] [6], since it maintains the temperature difference required by the monotonicity conditions between the evaporator and the condensation surface inside the HP and, in addition, contains the thermophysical characteristics of the HP in an implicit inverse form.

At the working fluid boiling beginning during a certain time interval, the temperature of the capillary-porous evaporator remains close to constant and with the continuation of heating and by solving the inverse problem of thermal conductivity, it becomes possible to calculate the heat capacity of the working evaporator and the heat of evaporation.

The mathematical description of the monotone heating mode contains and implies several simplifying assumptions, which as a result lead to analytical relations for the direct calculation of the IPTC.

Heating mode contains and implies several simplifying assumptions, which as a result lead to analytical relations for the direct calculation of the IPTC. However, it is necessary to introduce some specific adjustments to take into account several interfering factors. It is necessary to take into account the final longitudinal dimensions of the HP, which lead to a distortion of the HP's temperature field due to the heat exchange of the condensation end surface and the nearby side section with the cooling running water in the calorimeter, while analytical expressions imply the one-dimensionality of the temperature field in the HP.

The relatively large noticeable temperature differences within the HP during the boiling of the working fluid in the evaporator also require certain adjustments to the calculations. The values of the corrections will (can) be estimated in a special way.

The direct problem of the HP thermal conductivity is to find the HP's temperature (surface temperature for the thin HP's in a one-dimensional model of heat propagation in an adiabatic calorimeter) that satisfies the differential equation of thermal conductivity and has the specified boundary and initial conditions of unambiguity [9] [10] [11].

The solution of the direct problem for the HP's evaporator in the case of large temperature load and the boiling process beginning in the temperature region of the working fluid phase transition is accompanied by a nonlinear dependence of the intrinsic properties (heat capacity C_{HP} and thermal resistance R_{HP}) to temperature and leads to large error as the averaged results and the ambiguity of the resulting solutions.

At the same time, the average values of the obtained heat capacity results C_{HP} are not of great interest and make it absolutely necessary to isolate the zone of the HP's evaporator at the working fluid boiling beginning, thereby allocating the heat capacity C_{ev} of the HP's evaporative fragment.

The inverse problem of thermal conductivity (IPTC) in this case is to determine the parameters of internal heat transfer also in a one-dimensional model of heat propagation in an adiabatic calorimeter, the thermal resistance R_{HP} (or thermal conductivity λ_{HP}) and the heat capacity C_{ev} of a short linear HP's evaporator at high thermal loads and the working fluid boiling beginning.

IPTC is an incorrect problem in the sense of Hadamard [3] [4] [5] [6] [7], *i.e.* one whose numerical solution is unstable. This instability manifests itself in a significant and abrupt change in the solution itself with a small change in the initial conditions. To solve such problems, regularization methods have been developed and sustainable solutions have been proposed [9]-[13].

Formulation and solution of coefficient inverse problems of heat conduction in a one-dimensional coordinate system with one-dimensional temperature field are the theoretical basis of the main experimental methods for the evaporator's heat capacity study of short linear HP's (HP's evaporative fragment), using the results of thermal resistance measurement and the transferred heat power q_{ev} along the longitudinal axis to reflect a decrease in transmitted power due to losses on internal friction and heat transfer losses due to the nonabsolute adiabatic mode in the calorimeter [11] [12] [13] [14].

Thus, we have a coefficient inverse problem of thermal conductivity, when the known experimental data on the thermal resistance R_{HP} and the side surface temperature T_{HP} in adiabatic conditions, as well as the measured heat flow on the surface of the evaporator Q_{ev} (and condensation Q_{cond}), it is possible to restore the values of the heat capacity C_{ev} of the evaporative fragment depending on the temperature load δt.

2. Method and Materials

To conduct the experimental studies of the linear HP's thermal characteristics, we used previously developed and used in many previous studies short stainless steel HP's with a Laval nozzle-shaped vapour channel, the detailed description of which was repeatedly given in previous publications [16] [17] [18]. A schematic diagram of the experimental test setup is shown in **Figure 1**. In the upper cover capacitive sensors are installed to measure the working fluid condensate film thickness and temperature [19] [20] [21].

The capillary-porous evaporator 7 together with insert 4 forming a unified hydraulic working fluid delivery system, are made of layers of a thin stainless steel mesh with 0.07 mm thick each layer, with a cell size of 0.04 mm. The diethyl ether $C_4H_{10}O$ is used as the working fluid, which has the boiling temperature under the atmospheric pressure of T_B = 308.65 K (35.5˚C), freezing temperature T_F = 156.95 K (−116.2˚C) and critical parameters T_C = 466.55 K (193.4˚C), P_C =

3.61 MPa. The volume of the insertion pores is determined during manufacture, and in our case it is equal to 16.62×10^{-6} m^3, mass of diethyl ether with the density of 713.5 kg/m^3 (20˚C) in the insert pores is equal to 11.858×10^{-3} kg. The restriction in the HP's filling amount is made so that the evaporator is not flooded with ether at a high temperature load and the film boiling beginning on the lower cover surface of the HP (the evaporator surface).

The charging ratio of the HP with Laval-liked vapour channel (ratio of the diethyl ether volume to the total volume of the HP) is equal to 16.62×10^{-6} m^3/3.14×10^{-5} m^3 = 0.529.

The length of our HP's is $L_{HP} = 0.1$ m, diameter $d = 2 \times 10^{-2}$ m, when filling it with diethyl ether the average density is $\overline{\rho}_{HP} = 1.871 \times 10^3\ \mathrm{kg/m^3}$, $\overline{\rho}_{HP} \sim \rho_{ev}$, the average isochoric heat capacity $\overline{C}_{HP} = 1.15\ \mathrm{kJ/kg \cdot K}$ is a slightly varying temperature function due to the uniform distribution of the working fluid diethyl ether in the condensation, transport and evaporation areas of the HP and close to the total specific heat capacity $C_{eff}(T)$ of diethyl ether and stainless steel with the mass fractions of the components (2).

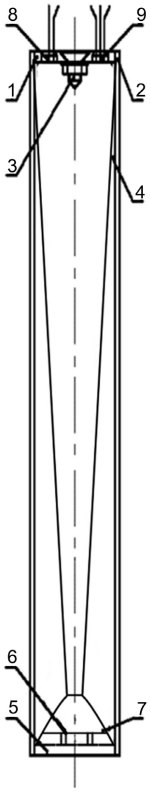

Figure 1. HP's diagram: 1: top cover; 2: cylinder body of the HP's; 3: locking element; 4: multilayer mesh capillary-porous insert with uniform dense radial cross-linking; 5: bottom cover; 6: capillary injector channels with a diameter of 1 mm; 7: bottom flat multilayer mesh evaporator. There are capacitance sensors 8, 9, 10 installed inside the top cover [16] [17] [18], two of which are intended for a condensate film thickness measurement, while the third with a welded on its electrodes microthermistor CT3-19 to measure the film temperature.

The defining parameter of the entire capillary-porous insert and the evaporator is a small longitudinal interlayer gap (clearance) between layers of the metal mesh, which does not exceed 0.007 mm, and developed by a porous system the capillary pressure, which is sufficient for the HP's work when the external inertial effects.

The last row of Table 1 shows the characteristics of a porous system, implemented in our HP's with a diethyl ether as a working fluid and the interlayer gap thickness is used as the average pore diameter.

The orientation of the longitudinal pores (clearances) with the liquid diethyl ether coincides with the skeleton wires of the capillary-porous insert and the direction of the heat flux propagation, therefore, the effective value of the thermal conductivity coefficient of a diethyl ether-saturated evaporator and insert can be calculated as follows:

$$\lambda_{ev} = \Pi \cdot \lambda_l + (1 - \Pi) \cdot \lambda_{sc}. \quad (5)$$

At the porosity value $\Pi = 0.72$ and values $\lambda_l = 0.136$ W/m K, $\lambda_{sc} = 24$ W/m·K, $\lambda_{ev} = 6.82$ W/m·K. The evaporator temperature T_{ev} (maximum value) is equal to the $T_{ev} = 329.75 \pm 0.01$ K (56.6˚C).

The measuring calorimeter for the HP's studies is shown in Figure 2. The external heat exchange surfaces of the HP's condensation zone are provided with insulated thermocouples and installed at a depth of 1 diameter in a vortex flow calorimeter with a stable water flow. To ensure accurate measurement of heat power and increase the HP's heat transfer coefficient, the jet stream of incoming water in the flow calorimeter is spun, the values of flow velocity and vorticity are recorded using air bubbles. The Reynolds number Re_{cal} in a calorimeter with water temperature $T_{cal} = (293 \pm 0.03)$ K is equal to $Re_{cal} = 3.68 \times 10^3$, Nusselt number $Nu_{cal} = 77.3$, heat exchange coefficient $a_{cal} = 2.4 \times 10^3$ W /m^2·K.

The HPs evaporators, also equipped with 0.1 mm diameter copper constantan wire thermocouples, is heated using a flat resistance heater, and the temperature is maintained at δT, K higher than the diethyl ether boiling temperature of 308.65 K under atmospheric pressure. The heater temperature is stabilized and HP's evaporators overheat value is set in the range of $\delta T = 0 \div 20$ K, herewith heat power of single HP does not exceed 200 W.

Table 1. Characteristics of the mesh wick with diethyl ether as a working fluid.

Average pore diameter, μ	Cell size, μ	The average diameter of the wire, μ	Porosity, %	The height of capillary rise of diethyl ether, mm	Permeability, K_{wick}, 10^{-10} m^2
120	400	15	78	8	7.25
30	30	10	72	81	0.2
7	30	10	72	400	0.15

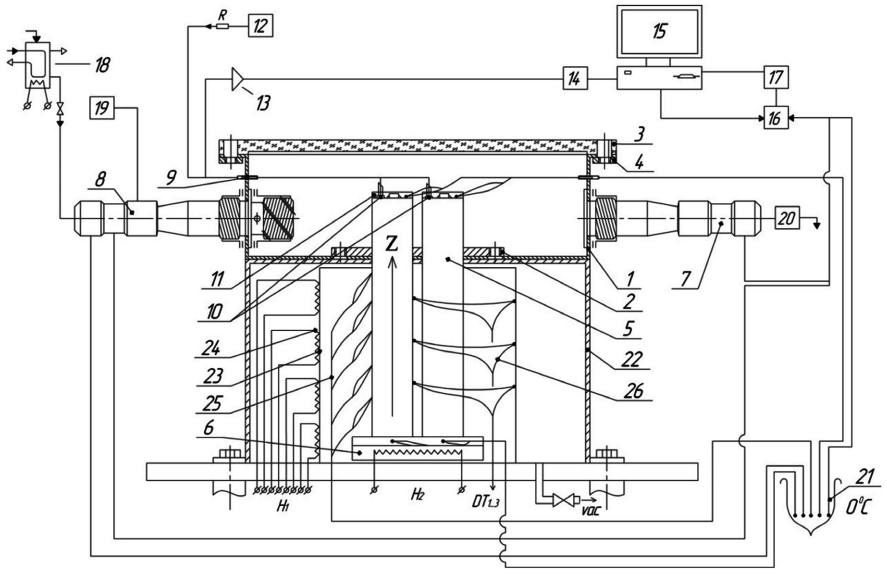

Figure 2. Scheme for the pulsation, heat conductivity and thermal resistance measuring of the short HP's in a vacuum adiabatic calorimeter, combined with a vortex flow calorimeter. 1: vortical continuous-flow calorimeter; 2: HP's bolting flange; 3: glass cover; 4: cover fastening; 5: HP's; 6: flat resistance heater; 7: outlet stub tube for water flow; 8: inlet stub tube swirler for water flow; 9: silicone sealant of the sensing wire; 10: capacitive sensors for measuring the thickness of the condensed layer of the working fluid; 11: the measuring and reference generators of the capacitive transducer; 12: external digital generator; 13: the amplifier; 14: digital oscilloscope; 15: computer; 16: commutation switch; 17: digital voltmeter; 18: container for constant water head; 19: source of air bubbles; 20: water flow meter; 21: vacuum-jacketed zero temperature container.

To reduce heat loss when working with HPs, they are placed in a stainless steel vacuum chamber 22 (10^{-3} torr), where they are further surrounded by thin-walled copper adiabatic screen 23, the inner surface of which is covered with a layer of nickel, and on the outer surface placed 4 sections guard heaters 24. The value of nonadiabaticity near the middle of the HP's does not exceed ~2×10^{-2} K, in the field of the resistive heater H_2 and HP's evaporators nonadiabaticity is about ~10^{-1} K.

The main HP, called measuring, is filled with diethyl ether and the reference one, which is completely identical to the main HP, is filled with dehumidified air at a pressure of 1 bar with dew point temperature lower than 233.15 K (−40˚C). The heat transfer coefficient K_{HP2} of the second HP does not exceed 0.15% from the first one (measuring one) K_{HP1} and is not taken into account. The second HP, completely identical to the first one, performing the reference function in measurements the condensate film thickness in the first HP [20] [21].

Conducted measurements of the condensate film thickness on the internal surface of the HP upper cover, using capacitive sensors and developed high frequency generators [16] [17] [18], give interesting results. Increased film thickness (and HP's high thermal resistance) at low temperature load and a sharp decrease in film thickness (and significantly reduced HP's thermal resistance) with increasing temperature load can be associated with a toroidal vapour vortex ro-

tation direction change [20] [21]. All the details of the indirect experimental confirmation of the vapour vortex rotation direction change near the flat condensation surface inside the HP's vapour channel and the condensate film thickness as a function of the temperature load are given in [16] [17] [18]. The results of condensate film thickness measuring are shown in **Figure 3**.

2.1. The Heat Balance Equation of the Evaporator

The most general and informative non-stationary energy equation for the work description of the HP's flat evaporator in the monotonous heating mode is the Fourier-Kirchhoff equation [5], which contains the isochoric heat capacity C_{ev}, J/kg·K, and the average evaporator density $\overline{\rho}_{ev}$, kg/m^3, the vapour and liquid phases flow velocity in vector form $\boldsymbol{v}$, m/s, inside the capillary-porous evaporator, dissipative functions Φ_{df}, the energy change as the moving vapour expands $P_{vp}\mathrm{div}(\boldsymbol{v})$, the increase in pressure P_{ev} in the vapour channel and without taking into account the mass diffusion fluxes as follows:

$$\begin{aligned} &C_{ev}\overline{\rho}_{ev}L_{ev}F(\overline{z})\left(\frac{\partial\overline{T}_{ev}}{\partial\tau}+\boldsymbol{v}\cdot\nabla T\right) \\ &=L_{ev}F(\overline{z})\left(\frac{\partial}{\partial\tau}+div(\boldsymbol{v})\right)P_{ev}+div(\lambda_{HP}\nabla T)+\sum_{i=1}^{i=2}\mu_i\Phi_{dfi} \end{aligned}. \quad (6)$$

The dimensionless length $\overline{z}$ and the average heat capacity C_{ev} of the HP's evaporator calculate in the usual way:

$$C_{ev}=C_{sc}+x_{ev}C_{vp}+(1-x_{ev})C_{fev}+C_w;\ \overline{z}=\frac{z}{L_{HP}}. \quad (7)$$

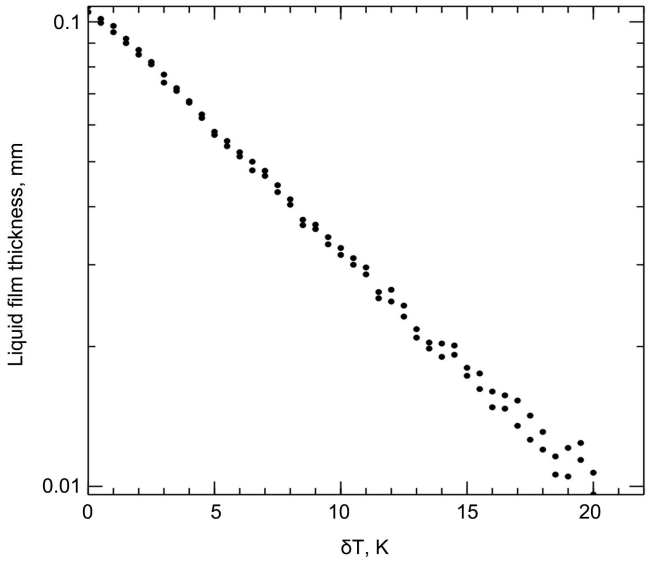

Figure 3. The average values of the diethyl ether film thickness on the HP's condensation surface, depending of the evaporator overheating $\delta T = T_{ev} - T_B$, K relative to the boiling point of the diethyl ether at atmospheric pressure, in a semi-logarithmic coordinate system.

With an increase in the temperature load in the initial heating period of a capillary-porous HP's mesh evaporator the wetting of the grid frame with diethyl ether deteriorates sharply, since the wetting angle increases with an increase in temperature. This effect is thermosensitive and already with a relatively small increase in temperature $\delta T = T_{ev} - T_B \sim$ (3 - 5) K wetting deteriorates, the level of diethyl ether in the grid evaporator decreases and further HP's heating $\delta T = T_{ev} - T_B \geq 10$ K through the flat surface of the bottom cover occurs in a thin layer of boiling diethyl ether.

The thickness of the diethyl ether layer decreases from ~3.5 mm at the heating beginning to the most intense boiling, while the vapour flow becomes stationary, and the thickness of the ether micro-layer does not exceed (1 - 2) × 10^{-2} mm. This fact greatly simplifies the conduct of assessments and the maximum achievable result in our conditions is as follows:

$$\begin{aligned} Q_{ev} &= -\lambda_{H2}\left(\frac{\partial T_{H2}}{\partial \bar{z}}\right)_{\bar{z}=0} = E_{H2} - C_{H2}\dot{T}_{ev} \\ &= \left(T_{H2} - \bar{T}_{fev}\right)F_{ev}(z)\Bigg/\left(\frac{\delta_c}{\lambda_c} + \frac{\delta_{wev}}{\lambda_w} + \frac{\delta_{fev}}{\lambda_{fev}} + \frac{1}{\alpha_{ev}}\right) = 118.4 \text{ W}. \end{aligned} \tag{8}$$

$$\begin{aligned} \Delta T_c &= \frac{Q_{ev}\delta_c}{\lambda_c F_{ev}} = 5.4 \text{ K}, \quad \Delta T_{wev} = \frac{Q_{ev}\delta_w}{\lambda_w F_{ev}} = 18.8 \text{ K}, \\ \Delta T_{fev} &= \frac{Q_{ev}\delta_{fev}}{\lambda_{fev} F_{ev}} = (35\ldots0.55)\text{K}. \end{aligned} \tag{9}$$

The equation of the thermal energy of a working HP's evaporator in a monotonic heating mode in the approximation of small heat losses $k_{HP}^{sh}\left(\bar{T}_{HP} - T_{shel}\right)$ in the adiabatic calorimeter can be represented using enthalpy equation as follows:

$$Q_{ev}(\tau) = H_{ev}(\tau) + \sum_{i=1}^{i=2}\mu_i\Phi_{dfi} + k_{HP}^{sh}\left(\bar{T}_{HP} - T_{shel}\right). \tag{10}$$

and the actual enthalpy equation of an evaporator in a monotonous heating mode also can be represented using this thermodynamic equation:

$$H_{ev}(\tau) = G_{vp}(\tau)r(T_B) + G_{vp}(\tau)C_{vp}\left(T_{ev} - T_{sc}\right) + G_l(\tau)C_{pl}\left(T_{ev} - \bar{T}_{fev}\right). \tag{11}$$

The expression for the thermal energy released in the HP's condensation region is written similarly using the heat balance equation:

$$\begin{aligned} Q_{cond} &= G_{vp}r(T_B)\frac{\mathrm{d}x_{ev}}{\mathrm{d}\bar{z}} + G_{vp}(1 - x_{ev})C_{vp}\frac{\mathrm{d}T_{fev}}{\mathrm{d}\bar{z}} + \lambda_{sc}(1 - \Pi)\frac{\mathrm{d}^2T_{sc}}{\mathrm{d}\bar{z}^2}F_{ev}(z)L_{ev} \\ &\quad - \sum_{i=1}^{i=2}\mu_i\Phi_{dfi} - k_{HP}^{sh}\left(\bar{T}_{HP} - T_{shel}\right). \end{aligned} \tag{12}$$

The performed measurements and calculations make it possible to estimate the heat transfer coefficient in the vortex flow calorimeter α_{cal} = 2.3 × 10^3 W/m^2·K, $\alpha_{cond} \geq 5 \times 10^3$ W/m^2·K, and the final expression for the maximum value of the condensation heat in our HP is the follows:

$$Q_{cond} = \left(\bar{T}_{fcond} - T_{cal}\right)F_{cond}\Bigg/\left(\frac{\delta_{fcond}}{\lambda_l} + \frac{\delta_w}{\lambda_w} + \frac{1}{\alpha_{cal}} + \frac{1}{\alpha_{cond}}\right) = 115.4 \text{ W}. \tag{13}$$

The thickness parameters in parentheses are equal to the following values:

$$\delta_{fcond} = 10^{-1} \text{ - } 10^{-3}\,\text{mm},\ \ \delta_w = 1\,\text{mm},$$
$$\alpha_{cal} = 2.4\times10^3\ \text{W/m}^2\cdot\text{K},\ \ \alpha_{cond} \geq (5\text{ - }10)\times10^3\ \text{W/m}^2\cdot\text{K}.$$

To solve the complex Fourier-Kirchhoff Equation (6), it is necessary first to determine the velocity field of the liquid and vapour phases in a capillary-porous evaporator using the Navier-Stokes equations. The results of this study will be presented later in a separate report.

To simplify all subsequent calculations, the average cross-section HP's temperature at any point at altitude $\bar{z}_i = z_i / L_{HP}$ inside the vapour channel can be considered equal to the surface temperature of the HP, measured at this height $T(\bar{z}_i, \tau)_{sur}$ in the vacuum chamber of the adiabatic calorimeter:

$$\frac{1}{F(\bar{z})}\int T_{HP}(\bar{z})\,\mathrm{d}F_i = T_{HP}(\bar{z}_i)_{sur} = T_{HP}(\bar{z}). \tag{14}$$

The vapour flow can be estimated according to the interphase mass transfer gives in case of small departures from equilibrium by the Hertz-Knudsen equation [22] [23]:

$$G_{vp} = \frac{2\xi}{2-\xi}\left(\frac{M}{2\pi R}\right)^{1/2}\left(\frac{P_{ev}}{\sqrt{\bar{T}_{fev}}} - \frac{P_{fcond}}{\sqrt{\bar{T}_{fcond}}}\right). \tag{15}$$

where the diethyl ether $C_4H_{10}O$, selected as the working fluid has a molar mass M = 74.1216 g/mol, R is the universal gas constant and ξ is the condensation coefficient, $\xi \leq 1$, defined as the ratio of the number of vapour molecules condensing over the total number of molecules which strikes the liquid film surface.

There is a redistribution of the liquid mass of diethyl ether inside the HP, while the heat capacity of the evaporator increases due to the liquid film boiling. In this case, the temperature T_{fev} of the diethyl ether layer and its dependence on time are determined using external thermocouples that control the temperature of the HP external surface inside the vacuum chamber. The results of the thermocouple measurements are shown in **Figure 4** and **Figure 5** in section 2.2.

2.2. Temperature Distribution Inside the Vapour Channel

Earlier calculations of the flow velocity and vapour density of diethyl ether using the Navier Stokes equation system in a short HP's vapour channel similar to the Laval nozzle [16] [18], allow us to calculate the temperature distribution in this channel. The ratio between the pressure, density and temperature of the condensing vapor in the first approximation can be given by the equation of state of an ideal gas in the following form [19] [20] [21]:

$$\rho_{vp}^{mix} = \frac{P}{RT};\ \ \frac{\rho_{vp}^{mix}}{\rho_v} = \left(\frac{P}{P_v}\right)^{1/k};\ \ P_v \sim P_{fcond};$$
$$\frac{P}{P_v} = \left[1 + \frac{k-1}{k}\frac{1}{RT_v}\left(\frac{u^2-u_v^2}{2} + \frac{v^2-v_v^2}{2m}\right)\right]^{k/(k-1)}. \tag{16}$$

where k = 1.31 is the value of the adiabatic index of diethyl ether vapour.

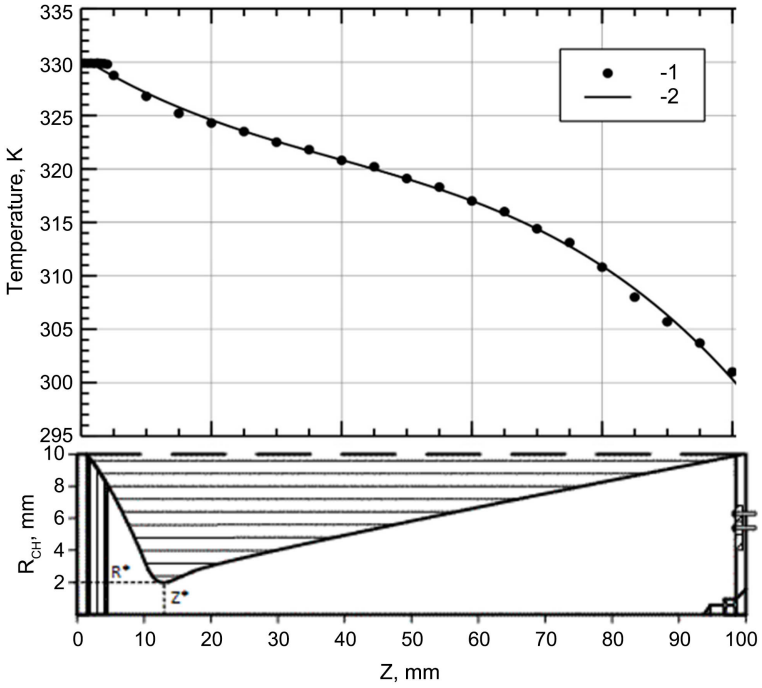

Figure 4. Comparison of the experimental values of the HP's surface temperature along the generatrix, and the calculated diethyl ether vapour temperature inside the Laval nozzle-liked formed vapour channel. **A**: is the upper part of the **Figure 4**. 1: black dots, the experimental values of the HP's surface temperature T_{sur} with a vapour channel made in the Laval nozzle-liked form, K; 2: the solid curve, the calculated temperature values T, K, in the Laval nozzle-liked formed HP's vapour channel. **B**: is the lower part of the **Figure 4**, which shows the half part of the vapour channel cross section along the longitudinal axis Oz.

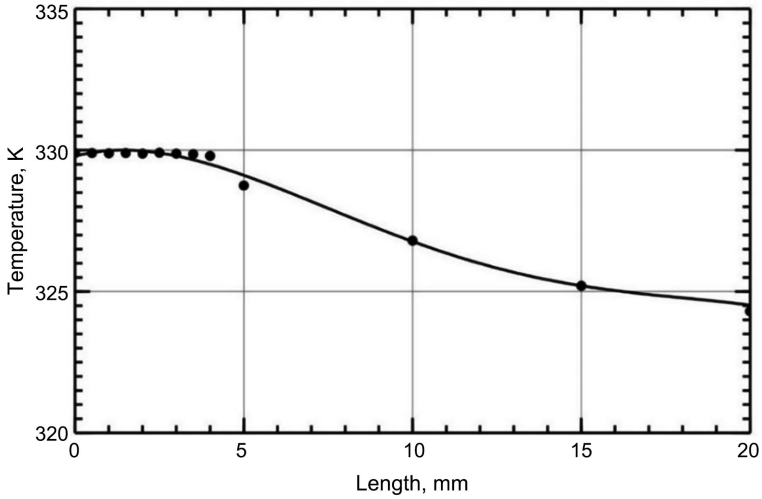

Figure 5. The experimental values of the HP's surface temperature of the evaporator with maximum filling by the diethyl ether at the boiling beginning on a large scale. It is clearly visible the weak evaporator temperature drop (<1 K) and a sharp drop of the vapour temperature inside the Laval nozzle-liked formed vapour channel above the evaporator, coinciding with the calculated vapour temperature values.

Calculations of moving vapour temperature in a short HP's vapour channel, made in the form of Laval nozzle, were performed using the program code ANSYS\CFD Fluent 6.3.26 -20090623 [24] and using Equation (16) and other more complete calculation equations given in [19] [20] [21]. Taking into account the tabular values [25] [26] [27] of the diethyl ether vapour pressure at the humidity coefficient γ_{dr} = 0.2, the temperature distribution inside the vapour channel along the longitudinal z axis was obtained at the beginning of boiling in the HP evaporator, as shown in **Figure 4** and **Figure 5** during overheating $\delta t = T_{ev} - T_B = 11$ K:

$$T = T_v \left(\frac{P}{P_v} \right)^{(k-1)/k}. \tag{17}$$

The calculated values of the vapour temperature along the longitudinal axis of the HP vapour channel at the temperature of lower layer of the diethyl ether in the evaporator $\overline{T}_{fev} = 329.75\ \mathrm{K}\left(56.6^{\circ}\mathrm{C}\right)$. The calculation error is 0.3%, the measurement error of the HP's surface temperature is less than 0.1 K. Heating and all calculations were carried out in the temperature range of the evaporator (298 - 348) K (25˚C - 75˚C).

The outer surface of the HP's body in the region of a 3.5 mm high multilayer mesh evaporator, filled with boiling diethyl ether is characterized by a close to constant temperature under monotonous heating, which is clearly seen in **Figure 4** and **Figure 5**. With further heating, the thickness of the diethyl ether layer in the evaporator and, accordingly, the width of the constant temperature region decreases.

Inside the vapour channel, the temperature decreases sharply, the temperature drop reaches ΔT = 35 K, due to the cooling in the condensation region and the influence of the Laval nozzle shape of the vapour channel. The results of the experimental analysis of the HP's surface temperature distribution along the generatrix also confirmed the nonlinear nature of the temperature distribution as a function of the channel length in the Laval-liked vapour channel.

Experimental data shows a close to constant temperature of the evaporator when diethyl ether boils in it, a weak nonlinearity in the confuser part of the nozzle, and a strong nonlinearity in the behavior of the temperature near the HP's condensation surface. With a further increase in the heat load, the length of the constant temperature region in the evaporator is reduced.

The results of numerical analysis of the vapour axial temperature distribution inside the Laval-liked HP's vapour channel of compressible moist vapour at high heat loads confirm the nonlinear character of the temperature distribution as function of the channel length, which is due to the joint influence of the channel shape in the form of a Laval-liked nozzle and a sharp gradient vortex formation near the HP's condensation surface, taking into account an additional temperature decrease inside the vortex ring of the condensing vapour [18] [21], which makes it extremely difficult to solve the heat equation for our HP's.

2.3. Thermal Resistance Results

Experimental values in the stationary state of the thermal resistance R_{HP} of a short HP's are defined as the thermophysical characteristic of the heat transfer device as a whole [28], at a constant value of the temperature load (pressure) on the evaporator $\delta t = T_{ev} - T_B$ and calculated using formula (18) and a vacuum adiabatic calorimeter, **Figure 2**, in which all parameters of the working HP, including temperature and transmitted thermal power, are measured using thermocouples.

The full temperature load on the evaporator $\delta t = T_{ev} - T_B$ = (0 - 20) K [16] (relative to the boiling point of ether at atmospheric pressure) is set and maintained using a precision temperature controller with a temperature step of δt = 0.5 K, the long-term instability does not exceed 1×10^{-2} K.

Experimental values of thermal resistance R_{HP} obtained during monotonic heating of the HP's evaporator with a speed close to linear in time 3×10^{-3} K/s using a special precision temperature controller and a system of computer-controlled switches, surface thermocouples, heater power measurements form arrays of data on HP surface temperatures in a vacuum adiabatic calorimeter, condensation surface, heater power E_{H2} and heat flows Q_{ev} and Q_{cond} for solving thermal conductivity equations and calculating thermal resistance according to formula (18) from [28]:

$$R_{HP}(t) = \frac{T_{ev} - T_{cond}}{Q_{ev}}. \tag{18}$$

The small size and the low heating rates ensured that the measurements of the R_{HP} were carried out under homogeneity conditions and local thermal equilibrium. The obtained values of the thermal resistance R_{HP}, K/W in the continuous heating mode refer to the direction of the heat flow that coincides with heat flow direction in the stationary states measurements.

The polynomial Equation (19) describing in dimensionless form the experimental values of the thermal resistance R_{HPk} for a time moment τ_k of the short HP with a Laval nozzle-liked vapour channel, depending on the overheating value of the evaporator δt: $0 \le \delta t \le 20$ (and also in dimensionless form) looks like this:

$$\begin{aligned} R_{HPk}(\delta t) &= \sum_{i=1}^{n_R} R_{HPki} (\delta t)^{i-1} \\ &= -2.0795621 \times 10^{-8} (\delta t)^7 + 1.6029662 \times 10^{-6} (\delta t)^6 \\ &\quad - 4.9921411 \times 10^{-5} (\delta t)^5 + 8.0489929 \times 10^{-4} (\delta t)^4 \\ &\quad - 0.0071936 (\delta t)^3 + 0.03633406 (\delta t)^2 \\ &\quad - 0.1113127 \delta t + 0.2702057, \ n_R \le 8 \end{aligned} \tag{19}$$

Standard deviation σ = 0. 0024929, Fisher criterion R^2 = 0.9980243.

The obtained experimental results of thermal resistance at temperature load δt > 10 K allow us to estimate the characteristic total thickness of the diethyl ether film on the evaporator surface (boiling in the evaporator) and the conden-

sation surface of short HP's with a Laval nozzle-liked vapour channel and flat upper and lower covers as follows (without the thermal resistance of covers):

$$\begin{aligned}\bar{\delta}_{ev}+\bar{\delta}_{cond} &\sim R_{HP}\lambda_l F\\ &= 4\times10^{-2}\ \mathrm{K/W}\times 0.136\ \mathrm{W/m^2\cdot K}\times 3.14\times10^{-4}\ \mathrm{m^2}\\ &\le 1.7\times10^{-6}\ \mathrm{m}.\end{aligned}$$

From the analysis of Figure (6), it follows that the film thickness on the evaporator is close to a constant value in the range of thermal loads δT = (10 - 20) K, and with a further increase in the temperature load δT, the evaporator begins to dry out and there is a sharp increase in the thermal resistance R_{HP}.

In addition, when the HP's evaporator is monotonically heated, the diethyl ether layer thickness inside the evaporator $\delta_{fev}(\tau)$ also decreases monotonically and within the range of the coordinate z:

$0 < z < L_{ev} = 0.035\cdot L_{HP}$ limited by the longitudinal dimensions of the evaporator L_{ev}, the functional dependence of the thermal resistance R_{HP} on the coordinate z: $R_{HP} = R_{HP}(z)$ is of practical interest, and has a positive sign:

$$\frac{\partial R_{HP}}{\partial z}=\frac{\partial R_{HP}}{\partial t}\left(\frac{\partial t}{\partial z}\right)=\frac{\partial R_{HP}}{\partial t}\left(\frac{\partial z}{\partial t}\right)^{-1}>0;\ \ 0\le z<L_{ev}=0.035\cdot L_{HP}. \tag{20}$$

The distributions of the experimental values of the HP's surface temperature shown in Figure 4 and Figure 5 ($(\partial t/\partial z) < 0$) at the diethyl ether boiling beginning in a saturated evaporator under the monotonic heating, and the decreasing values of the thermal resistance on a global evaluation between evaporator and condenser ($(\partial R_{HP}/\partial t) < 0$) in Figure 6, show a positive value of the derivative in Equation (21). And this authorizes the hypothesis that the thermal resistances R_{HP} associated with each z position $0 < z < L_{ev}$ confirms the dependence on $R_{HP} = R_{HP}(z)$ and apply it in the thermal conductivity equation. The same can be said or concluded about the heat capacity of the evaporator.

3. Mathematical Model of the Inverse Thermal Conductivity Problem

Let's formulate a mathematical statement of the inverse problem of restoring the heat capacity of working HP's. Let there be a vertically oriented HP with the length L_{HP} = 100 mm and diameter of 20 mm, $D_{HP}/L_{HP} \le 0.2$ and the temperature field inside can be viewed in one-dimensional axisymmetric mode and located at the bottom of HP the capillary-porous evaporator with a thickness of $L_{ev} = 0.035\cdot L_{HP}$. At the lower end of the HP the evaporator is supplied with a flow of heat $Q_{ev}\left(\bar{z}=0\right)$ from a flat heater H_2, Figure 2. At the upper end of the evaporator there is a heat exchange $Q_{ev}\left(\bar{z}=0.035\right)$ and at the upper HP's end there is a heat exchange $Q_{ev}\left(\bar{z}=1\right)=Q_{cond}$ with an external fluid with a constant temperature T_{cal}.

The classical equation of spatial thermal conductivity for the linear HP's as a solid rod (solid body) is looks like this [4] [5] [6]:

$$\rho_{HP}c_v\left(t\right)L_{HP}F\left(\bar{z}\right)\frac{\partial T}{\partial\tau}=div\left(\lambda_{HP}grad\,T\right). \tag{21}$$

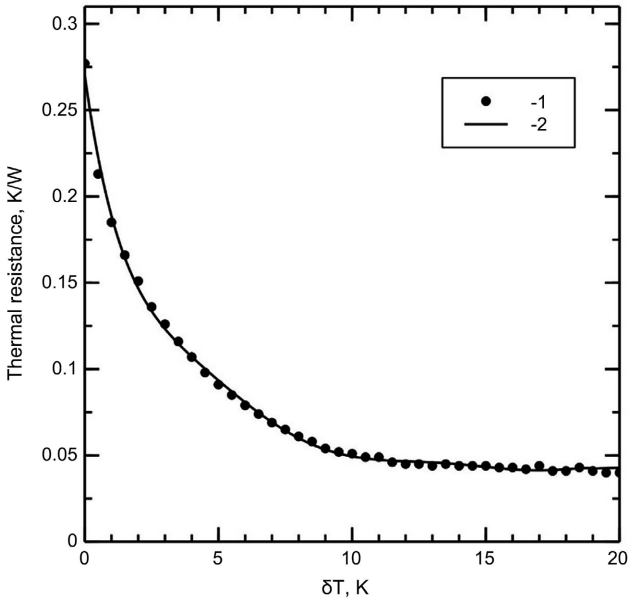

Figure 6. Thermal resistance R_{HP}, depending on the evaporator overheating $\delta t = T_{ev} - T_B$ relative to the boiling point of diethyl ether at atmospheric pressure. 1: black dots, experimental stationary R_{HP} values of short HP's with a vapour channel made in the Laval nozzle-liked form; 2: solid lines, the experimental values of the thermal resistance R_{HP} of the same HP obtained in the continuous heating mode with close to linear in time speed of 3×10^{-3} K/s.

In a working HP with monotonous heating the heat capacity C_{ev} of the evaporator can be considered and analyzed only as the heat capacity of the HP's lower fragment $C_{ev} = C_{HP}\left(\overline{z} = 0.035\right)$ with a thickness of $L_{ev} = 0.035 \cdot L_{HP}$ and thermal resistance $R_{ev} = R_{HP}\left(\overline{z} = 0.035\right)$.

The distribution of the one-dimensional axisymmetric temperature field $t_{HP}\left(\overline{z}_i\right)_{sur}$ and $\dot{t}\left(\overline{z}, \tau_k\right)_{sur}$ along the longitudinal dimensionless $\overline{z}$ -axis of a short linear HP's is used to solve the heat conduction Equation (22) for the evaporator fragment without internal sources [4]:

$$\frac{1}{\overline{z}} \frac{\partial}{\partial \overline{z}} \frac{1}{R_{ev}(t)} \frac{\partial t\left(\overline{z}, \tau\right)}{\partial \overline{z}} = C_{ev}(t) \dot{t}\left(\overline{z}, \tau\right); \ \overline{z} = \frac{z}{L_{HP}} \le 0.035. \tag{22}$$

The thermal resistance of the evaporator (evaporative HP fragment) is an integral part of the thermal resistance R_{HP} of the entire HP, and the value of the thermal resistance of the evaporator during the diethyl ether boiling at temperature load (pressure) > 11 K can be estimated using the experimental results presented in **Figure 6**. Given the close thicknesses of diethyl ether films in the evaporator and on the condensation surface of HP $\overline{\delta}_{ev} \sim \overline{\delta}_{cond}$ during film boiling, the thermal resistance of the evaporator (evaporative fragment) will be no more then $R_{ev} \le 0.02$ K/W.

Energy losses due to friction in the vapour channel and non-absolute calorimeter adiabaticity lead to the fact that the thermal power of Q_{ev} and Q_{cond} differ from each other:

$$\left(Q_{ev}-Q_{cond}\right)/Q_{ev}\le 2.6\%\,.$$

And the heat power becomes a function of the dimensionless vertical coordinate $\bar{z}$ and time with monotonous heating:

$$Q_{ev}=Q_{ev}\left(\bar{z},\tau\right). \tag{23}$$

One of the possible formulations of the coefficient inverse problem (CIP) for Equation (23) consists in setting redefined boundary conditions, with the help of which the definition unicity of three functions – temperature $t_{sur}\left(\bar{z},\tau_k\right)$, heat capacity $C_{ev}\left(\bar{z},\tau_k\right)$ and thermal resistance $R_{ev}\left(\bar{z},\tau_k\right)$ (or thermal conductivity $\lambda_{ev}\left(\bar{z},\tau_k\right)$), moreover all functions must be analytical functions, for example, represented as polynomials or piecewise smooth spline functions. For experimentally determined boundary conditions, the inverse heat conduction problem for Equation (22) is usually incorrect in the classical sense [9] [10] [11]. To bring it to a conditionally correct formulation, we restrict the class of acceptable solutions to a set of piecewise regular approximating dependencies and apply the step – by step principle of natural regularization for IPTC solution [6] [9].

The temperature distribution of the cylindrical HP's housing inside the vacuum chamber with an adiabatic shell near the flat resistive heater is symmetrical:

$$\left[\frac{\partial t\left(\bar{z},\tau\right)}{\partial x}\right]_{\bar{z}=0}=\left[\frac{\partial t\left(\bar{z},\tau\right)}{\partial y}\right]_{\bar{z}=0}=0\,. \tag{24}$$

The initial boundary conditions [29] [30] [31]:

$$t\left(0,\tau\right)\equiv t_{ev}=T_{ev}\left(\tau\right)-\left(R_c+R_w+R_{fev}\right)Q_{ev}\left(\tau\right). \tag{25}$$

$$t\left(0,0\right)=t_0;\;\; t\left(0,\tau_k\right)=t_0+\tau_k\times 3\times 10^{-3}\ \mathrm{K/s}\,. \tag{26}$$

$$t\left(L_{HP},\tau_k\right)\equiv t_{cond}=T_{cond}\left(\tau_k\right)+\left(R_{cal}+R_w+R_{fcond}+R_{cond}\right)Q_{cond}\left(\tau_k\right). \tag{27}$$

$$Q_{ev}\left(\bar{z}=0,\tau_k\right)=E_{H2}-C_{H2}\dot{T}_{ev}\left(\bar{z},\tau_k\right). \tag{28}$$

The Q_{cond} energy transmitted by HP to the vortex flow calorimeter during vapour condensation is determined using the experimental stand shown in **Figure 2** and Equation (13).

We write down the dimensional equation of thermal conductivity to estimate the heat capacity of a capillary-porous evaporator with a finite height of $0.035\cdot L_{HPi}$ in the following standard form:

$$zC_{evk}\left(t\right)\dot{t}\left(z,\tau_k\right)=\frac{\partial}{\partial z}\left[\frac{L_{HP}}{R_{HP}\left(t\right)F\left(z\right)}\frac{\partial t\left(z,\tau_k\right)}{\partial z}\right];\;\frac{z}{L_{HP}}\le 0.035\,. \tag{29}$$

And we introduce a general expression for the heat flow $q\left(z,\tau_k\right)$ inside the short HP along the longitudinal z axis:

$$q\left(z,\tau_k\right)=z\lambda_{HP}\frac{\partial T_{HP}\left(z,\tau_k\right)}{\partial z}=z\frac{L_{HP}}{R_{HP}F_{HP}}\frac{\partial T_{HP}\left(z,\tau_k\right)}{\partial z}=E_{H2}-C_{H2}\dot{T}_{ev}\left(z,\tau_k\right). \tag{30}$$

In the first approximation, in which the heat flow is determined only by the

HP's capillary-porous evaporator without taking into account heat losses, the heat propagation equation in the vapour channel using the thermal resistance R_{HP} of a short HP's as a whole can be written in the following form:

$$\begin{aligned} & z\frac{L_{HP}}{R_{HP}(t)F_{ev}}\frac{\partial T_{HP}(\bar{z},\tau_k)}{\partial \bar{z}} \\ & = G_{vp}r(T_B)\frac{\mathrm{d}x_{ev}}{\mathrm{d}\bar{z}} + G_{vp}C_{vp}\frac{\mathrm{d}T_{fev}}{\mathrm{d}\bar{z}} + \lambda_{sc}(1-\Pi)\frac{\mathrm{d}^2T_{sc}}{\mathrm{d}\bar{z}^2}F_{ev}(z)L_{ev}. \end{aligned} \tag{31}$$

The solution of the Equations (29) and (31) is possible only with positive values of time τ_k and heat capacity $\bar{C}_{evk}(T)$:

$$\tau_k > 0;\ \bar{C}_{evk}(T) > 0$$

To simplify all subsequent calculations, it is possible to take the initial temperature value equal to zero:

$$t(\bar{z},0) = 0$$

Equations (30) and (29) of the heat flow propagation $q(z,\tau_k)$ can be rewritten in the dimensionless form $q_{ev}(\bar{z},\tau_k)$ as the heat flow of the evaporator (without taking into account heat losses) along the *z*-axis at time moment τ_k and presented as a system of two energy equations for calculating the heat capacity $C_{evk}(t)$ and the heat flow of the evaporator $q_{ev}(\bar{z},\tau_k)$, the value of which is related to the thermal resistance R_{HP} of a short HP's as a whole and for the time τ_k can be represented as follows:

$$\bar{z}C_{evk}(t)\dot{t} + \frac{\partial q_{ev}(\bar{z},\tau_k)}{\partial \bar{z}} = 0. \tag{32}$$

$$z\frac{L_{HP}}{R_{HP}F(\bar{z})}\frac{\partial t(\bar{z},\tau)}{\partial \bar{z}} + q_{ev}(\bar{z},\tau_k) = 0. \tag{33}$$

The values of the variable thermal power $q_{ev}(\bar{z},\tau_k)$ on the lower HP's flat borders, on the upper boundary of the flat evaporator and on the upper flat borders are equal to:

$$q_{ev}(0,\tau_k) = Q_{ev};\ q_{ev}(0.035,\tau_k) = Q_{0.035};\ q_{ev}(1,\tau_k) = Q_{cond}. \tag{34}$$

and Equation (33) for determination the transmitted thermal power by the HP's capillary-porous evaporator at a height of $z = 0.035 \cdot L_{HP}$ is made using the HP's surface temperature distribution in the adiabatic calorimeter:

$$\begin{aligned} q_{ev}(\bar{z}=0.035,\tau_k) &= -z\frac{L_{HP}}{R_{HP}F(\bar{z})}\left[\frac{\partial t(\bar{z},\tau)}{\partial \bar{z}}\right]_{\bar{z}=0.035} \\ &= -0.035\frac{L_{HP}^2}{R_{HP}F(\bar{z})}\left[\frac{\partial t(\bar{z},\tau)}{\partial \bar{z}}\right]_{\bar{z}=0.035}. \end{aligned} \tag{35}$$

The heat capacity of the evaporator allows us to evaluate the work of the HP. To calculate the

HP's evaporator heat capacity C_{evk}, the heat output in the evaporator volume can be considered as reduced by the temperature reduce from the Equation (31)

and (35), and an illustration of the experimental temperature distribution data from Figure 4 and Figure 5:

$$0.035C_{evk}(t)\dot{t} = -\left[\frac{\partial q(\bar{z},\tau_k)}{\partial \bar{z}}\right]\Bigg|_{\bar{z}=0.035}. \quad (36)$$

Figure 4 and Figure 5 show the close to the constant experimental temperature distribution inside the evaporator with boiling diethyl ether at a high heat load and further temperature drop in the HP's Laval nozzle-liked vapour channel up to the condensation surface.

3.1. Performing Calculations of the Inverse Thermal Conductivity Problem

The inverse thermal conductivity problem (ITCP) solution for the HP's evaporator is a method of stepwise continuation of the known solution, for example equal to zero at the initial moment, for the next time interval $\Delta\tau_k = (\tau_k, \tau_{k+1})$ and the corresponding temperature interval $t_k = (t_k, t_{k+1})$ to calculate the heat capacity of a capillary-porous evaporator with a height (thickness) of $0.03 \cdot L_{HP}$.

The solution of the equations system (32) and (33) is carried out using experimentally determined surface temperature values $t(\bar{z},\tau_k)$ in the range $HP_{0.03} = (\tau_k, \tau_{k+1}) \times (0, 0.035 \cdot L_{HP})$, experimental thermal resistance values $R_{HP}(\bar{z},\tau_k)$ in the range $HP_1 = (\tau_k, \tau_{k+1}) \times (0, 1 \cdot L_{HP})$, and calculated values of the evaporator volumetric heat capacity $C_{evk}(\delta t)$ in the range $(\tau_k, \tau_{k+1}) \times (0, 0.035 \cdot L_{HP})$ and satisfying the thermal conductivity equations (22) and additional conditions (25) - (28), provided that the thermal resistance defined in stationary states is known as a polynomial (19).

Crank-Nicholson calculation scheme, Figure 7 with temperature averaging on the previous calculation layer and taking into account the temperature dependence of the thermal conductivity coefficient can be used to improve the calculations accuracy. The equation for the Crank-Nicholson scheme calculation of the evaporator heat capacity is as follows:

$$\rho_{evi}C_{evi}\frac{T_i^{n+1}-T_i^n}{\Delta\tau} = \lambda_{evi}\left(\frac{T_i^{n+1}+T_i^n}{2}\right)\left(\frac{T_{i-1}^{n+1}-2T_i^{n+1}+T_{i+1}^{n+1}}{2h^2}+\frac{T_{i-1}^n-2T_i^n+T_{i+1}^n}{2h^2}\right). \quad (37)$$

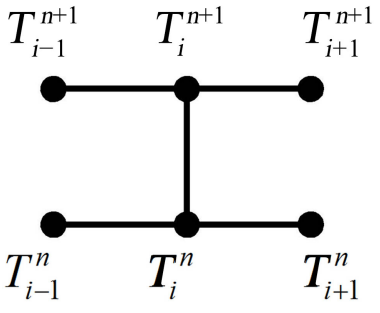

Figure 7. A six-point difference scheme in which three points are taken from the next (new) time layer $n + 1$, and three from the old (previous) time layer n.

The coefficient λ_{evi} of the evaporator thermal conductivity can be estimated by the Equation (5).

Experimental temperature t_k at time τ_k inside the HP's vapour channel with monotonous heating relative to the boiling point t_B of diethyl ether at atmospheric pressure is determined as follows:

$$t_k = t\left(\overline{z}, \tau_k\right) = \delta t\left(\overline{z}, \tau_k\right) + t_B;\ \ \delta t_k = \delta t\left(\overline{z}, \tau_k\right) = t_k - t_B. \tag{38}$$

At the initial time moment τ_k and at the initial temperature value t_k, we should consider that the HP's evaporator heat capacity $C_{evk}(\delta t)$ with the initial temperature load value $\delta t\left(\overline{z}, \tau_k\right)$ are known and is equal zero, so the heat capacity from now on further heating can be represented as a polynomial with a variable (δt):

$$C_{evk}\left(t\right) = \phi\left(\xi\right) \cdot \sum_{i=1}^{n_c} C_{evki}\left(\delta t\right)^{i-1};\ \ n_C \le 10. \tag{39}$$

Approximation function $\Phi(\xi)$ is a mandatory regularizing parameter in the form of monotone increasing function, $\Phi(\xi) = \xi$, or maybe $\exp(\xi)$. The value of numerical parameter $\Phi(\xi)$ determines the stability and the range of acceptable heat capacity properties, and smoothes out non-linearity's in a blurred thermal transformation in the HP's evaporator. With the change from linear to an exponential dependence, the error in calculating the heat capacity decreases markedly, especially when the polynomial heat capacity function leaves the peak, see **Figure 8**. This is due to the fact that $\exp(\xi)$ provides a limit on the range of HP's permissible properties in a positive value with C_{evk} and $R_{HPi}(\lambda_{HPi}) > 0$, and the solution for C_{evk} is significantly much improved, especially at the exit from the heat capacity peak, corresponding to the blurred phase transition at the boiling beginning in the HP's evaporator. In the case of $\Phi(\xi) = \xi$, the error in the heat capacity recovery in the temperature range (298 - 348) K (25˚C - 75˚C) reaches 25%, and when replaced by $\exp(\xi)$ falls to 2%.

The temperature time derivative is a constant value for time values $\tau > \tau_k$ and is a coordinating (synchronizing) parameter of all measurements in a time interval $\Delta\tau_k$:

$$\begin{aligned} &\dot{t}_i > 0,\ i = 0, \cdots, 2,\ \ \tau > \tau_k;\ \ t_k = t_0 + \tau_k \times 3 \times 10^{-3}\ \mathrm{K/s};\\ &\Delta t_k = \Delta\tau_k \times 3 \times 10^{-3}\ \mathrm{K/s}. \end{aligned} \tag{40}$$

The experimental distribution of the HP's surface temperature t_k at time τ_k along the HP's body is known, are positive and can be written as follows:

$$\begin{aligned} &t_{ev}\left(\tau_k\right) = t_{k0}\left(\overline{z} = 0\right) > 0;\ \ t_{0.035}\left(\tau_k\right) = t_{k0}\left(\overline{z} = 0.035\right) > 0;\\ &t_1\left(\tau_k\right) = t_{k0}\left(\overline{z} = 1\right) > 0. \end{aligned} \tag{41}$$

The accounting and synchronization of the thermal resistance R_{HPk} equilibrium values (33) in a linear slow heating process to the moments of time measurements τ_k is performed using the value of the temperature load δt_k from (38) and (40)-(41). The thermal power from the Equation (30) is calculated as follows:

$$\tau > \tau_k : Q_{\overline{z}=0}\left(\tau_k\right) = Q_{ev};\ Q_{\overline{z}=0.035}\left(\tau_k\right) = q_{\overline{z}=0.035};\ q_{\overline{z}=1}\left(\tau_k\right) = Q_{cond}. \tag{42}$$

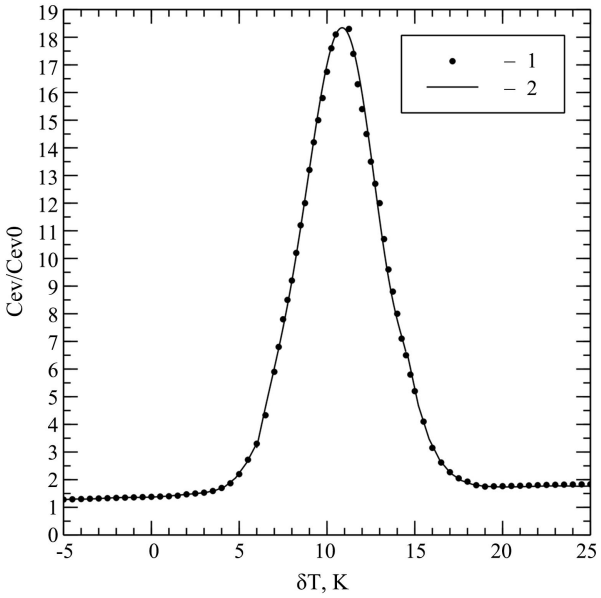

Figure 8. The calculated values of the HP's evaporator heat capacity C_{ev}/C_{ev0}: C_{ev}, the heat capacity of the diethyl ether-saturated evaporator, J/K; C_{ev0}, the heat capacity of the reference HP evaporator filled with dried air, J/K. 1-black dots, values of the relative heat capacity of the HP's evaporator with a Laval nozzle-shaped vapour channel, obtained by solving the inverse problem using Equation (44) with a temperature step of 0.5 K. $\delta t = T_{ev} - T_B$, when the diethyl ether boiling process begins; 2-a polynomial function of the tenth degree for smoothing the obtained points of the evaporator heat capacity.

When the ITCP problem at time τ_k is solved and the temperature at time τ_{k+1} of the evaporator $\bar{z} = 0$: $t_{ev}(\tau_k) = t_{k0}(\bar{z} = 0)$, at a height $\bar{z} = 0.035$: $t_{0.035}(\tau_k) = t_{k0}(\bar{z} = 0.035)$ and the temperature of the HP condensation surface $\bar{z} = 1$: $t_1(\tau_k) = t_{k0}(\bar{z} = 1)$ becomes measured and known, this solution becomes the temperature and thermal power initial distribution at transition to the next τ_{k+1} time interval, $\Delta\tau_{k+1} = (\tau_{k+1}, \tau_{k+2})$. From the solution of the problem on the time interval $\Delta\tau_{k+1}$, the function $C_{k+1}(t)$ is determined on the temperature interval $t_{k+1} = (t_{k+1}, t_{k+2})$.

To reduce the number of C_{k+1} parameters, defined at each time interval $\Delta\tau_{k+1}$, the crosslink should be performed with the polynomial (39) from the previous calculation at the boundary point of the temperature t_k by the function and its derivatives, this greatly simplifies all calculations.

The total number of equations for crosslinking $N_c = 2$ (heat capacity and temperature derivative of heat capacity), and the maximum degree of the polynomial $n_c = 10$ are primarily the main regularizing parameters of calculation, and were determined in accordance with the estimated accuracy of the heat capacity and experimental error of the temperature measuring.

In addition, the method of numerical solution of ITCP for short linear HP's using a polynomial expansion of the heat capacity, the size of each time $\Delta\tau_k$ step is an important regularizing parameter [12] [13] [14] [15] [32] [33]. The optimal

time step size $\Delta\tau_k$ is the determining parameter of the calculations accuracy, depends on many HP's parameters, and it was chosen experimentally. The characteristic time of all measuring sensors survey of the experimental stand, **Figure 2** is $\Delta\tau_{meas}$ = 21 s, so the time step $\Delta\tau_k$ in the area of boiling beginning of the diethyl ether in the HP evaporator changed from $\Delta\tau_k$ = 30 s up to $\Delta\tau_k$ = 60 s, and the temperature step reached the value of $\Delta t_k \le 0.2$ K. In the initial heating region the temperature step could be greater and reached the value of $\Delta t_k \le 0.5$ K.

The program that controls the operation of the measuring stand, **Figure 2**, has two operating modes: "control" and "measurement". In the "control" mode, all sensors are cycled, including thermocouples, thermistors, capacitive sensors, controls the power of the main resistive heater and protective heaters of the adiabatic calorimeter system, the regime of "zero heating" mode of the HP's evaporator is specified, the measurement results are processed and output on the display screen.

In this mode, the parameters of the control program are specified such as the duration of the sensors readings measurement, the measurement times of digital voltmeters, oscilloscopes, frequency meters, etc. After the HP evaporator and the vortex flow calorimeter reach stationary isothermal states, the program switches to the "measurement" mode.

The main resistive heater H_2 and control system are switched on, and the linear time heating of the HP's evaporators begins, the adiabatic system and all measuring sensors start working. In this mode, the temperatures distribution on the outer surface of the measuring HP, the evaporator heat power, the condensation surface temperature, the heat output of the adiabatic system and all other thermal characteristics, including the heat transfer characteristics of the HP, are measured. The obtained experimental data arrays are saved and a measurement library is formed.

3.2. Performing Calculations of the Evaporator Heat Capacity

We analyze the case when the thermal resistance R_{HP}, Equation (19) of the entire HP as a whole is known, have a positive value and it is necessary to calculate the heat capacity of a capillary-porous evaporator with a height of 3.5 mm and saturated with diethyl ether. We integrate Equation (22) with respect to $\bar{z}$ and, taking into account the experimental boundary conditions (25), (26), (27) and (28) we obtain a nonlinear integral equation for calculating the evaporator heat capacity at the time moment τ_k:

$$\int_0^{0.035} \bar{z} C_{evk}(t)\dot{t}(\bar{z},\tau_k)\mathrm{d}\bar{z} = 0.035 q_{ev}(\bar{z},\tau_k). \tag{43}$$

To solve such integral equations, the finite difference method is used, based on replacing the derivatives with their approximate values expressed in terms of the functions differences at individual discrete points (nodes) of the finite-difference grid, Equation (37).

We will solve the functional Equation (43) by the iterative method, for which

it is necessary to proceed to the variational formulation of this task. We define the target functional as the discrepancy, corresponding to the difference between the left and right sides of Equation (43), and the calculation problem for each time interval $\Delta\tau_k$ will look like the task of minimizing the discrepancy functional:

$$\begin{aligned}\sum\nolimits_k \delta C_{evk}(t) &= \frac{1}{2}\sum\nolimits_k \int_{\tau_k}^{\tau_{k+1}} \left[\int_0^{0.035} \bar{z} C_{evk}(t)\dot{t}(\bar{z},\tau_k)\,\mathrm{d}\bar{z} - 0.035 q_{ev}(\tau_k)\right]^2 \mathrm{d}\tau \\ &= \inf C_{evk}^i(t).\end{aligned} \tag{44}$$

The most suitable way to minimize the functional is the conjugate gradient method [34] [35] [36]. To calculate the gradient components of the functional (44) (Frechet derivatives) at the points of minimizing sequence, the method of the optimal process control theory [35] [36] is used, described by partial differential equations [35]. In this method, an important role is played by the so-called conjugate boundary value problems corresponding to the original optimal control problem.

The Lagrange functional **L** for minimization the problem (44) with additional conditions (22), (25), (26) and with the values of the heat flow at the boundaries of the evaporator (32), (36) is as follows:

$$\begin{aligned}\mathbf{L} = &\left[\frac{\partial \sum_k \delta C_{evk}(t)}{\partial c_i}\right] + \int_{\tau_k}^{\tau_{k+1}} \left[\int_0^{0.035} \eta\left(\bar{z} C_{evk}(t)\dot{t} + \frac{\partial q(\bar{z},\tau_k)}{\partial \bar{z}}\right)\right] \mathrm{d}\bar{z}\,\mathrm{d}\tau_k \\ &+ \int_{\tau_k}^{\tau_{k+1}} \left[\int_0^{0.035} \chi\left(q_{ev}(\bar{z},\tau_k) + z\frac{L_{HP}}{R_{HP}F(\bar{z})}\frac{\partial t(\bar{z},\tau)}{\partial \bar{z}}\right)\right] \mathrm{d}\bar{z}\,\mathrm{d}\tau_k.\end{aligned} \tag{45}$$

where the domain of variables τ_k and $q_{ev}(\bar{z},\tau_k)$ is kept the same as $\mathrm{HP}_{0.035}$ and HP_1, and η and χ are Lagrange multipliers corresponding to the first and second Equations (32) and (33).

To obtain the gradient expression of the functional **L** [35], Lagrange multipliers and formulate the conjugate task of calculating the heat capacity, we present a variation of the Lagrange function with respect to the variables τ_k and $q_{ev}(\bar{z},\tau_k)$ and the heat capacity parameters $C_{evk}^i(t)$, and taking into account the boundary conditions (25) and (26) and the initial conditions (32), (33), (40) and expressions for the heat flow (30), (35):

$$\begin{aligned}\delta\mathbf{L} = &\sum\nolimits_i \int_{\tau_k}^{\tau_{k+1}} \left[\int_0^{0.035} \chi C_{evk}^i(t) g_i \delta\left(\bar{z}\frac{L_{HP}^2}{R_{HP}F(\bar{z})}\right)\right] \mathrm{d}\bar{z}\,\mathrm{d}\tau_k \\ &- \int_{\tau_k}^{\tau_{k+1}} \left[\int_0^{0.035} \left(\bar{z} C_{evk}^i(t)\dot{\eta} + \bar{z}\frac{L_{HP}^2}{R_{HP}F(\bar{z})}\frac{\partial b}{\partial \bar{z}}\right)\right] \delta t\,\mathrm{d}\bar{z}\,\mathrm{d}\tau_k \\ &- \int_{\tau_k}^{\tau_{k+1}} \left[\int_0^{0.035} \left(\frac{\partial \eta}{\partial \bar{z}} - \bar{z}\chi\right)\right] \delta q_{ev}(\bar{z},\tau_k)\,\mathrm{d}\bar{z}\,\mathrm{d}\tau_k + \int_0^{0.035} \bar{z}\eta C_{evk}^i(t)\,\delta t\,\mathrm{d}\bar{z} \\ &+ \int_{\tau_k}^{\tau_{k+1}} \left[\bar{z}\frac{L_{HP}^2}{R_{HP}F(\bar{z})} - \int_0^{0.035} \bar{z}\eta C_{evk}^i(t)\dot{t}(\bar{z},\tau_k)\,\mathrm{d}\bar{z} - 0.03 q_{ev}(\tau_k)\right] \delta t\,\mathrm{d}\tau_k.\end{aligned} \tag{46}$$

where the value g_k denotes the derivative of the heat capacity components in the

following form:

$$g_i = \frac{\partial C_{evk}(t,\tau_k)}{\partial C^i_{evk}(t,\tau_k)};\ \frac{\partial \sum_k \delta C_{evk}(t)}{\partial C^i(t,\tau_k)} = \int_{\tau_k}^{\tau_{k+1}} \left[\int_0^{0.035} \eta \dot{t}(\bar{z},\tau_k) g_i \right] \mathrm{d}\bar{z}\mathrm{d}\tau_k . \quad (47)$$

where η, is the solution of the conjugate problem completely corresponding to the original problem (22), (25) and (27). In the reverse time, $\tau = \tau_{k+1} - \tau_k$ the conjugate problem is written using Equations (32) and (33) and the HP's thermal conductivity coefficient a^k:

$$\bar{z}\eta_k = a^k \frac{\partial(\bar{z}\partial\eta_k/\partial\bar{z})}{\partial\bar{z}};\ a^k = \frac{\lambda_k}{C_{evk}(t,\tau_k)} = \frac{1}{C_{evk}(t,\tau_k)} \frac{L_{HP}}{R_{HPk}F(\bar{z})} . \quad (48)$$

Both the initial and boundary conditions of the conjugate task are written in the usual way, and at the upper boundary of the evaporator, the conjugate value is equal to the caloric residual from the square brackets in the Equation (44):

$$\eta(\bar{z},0) = 0;\ \eta(0,\tau_k) = 0 .$$

$$\eta(\bar{z} = 0.035,\tau_k) = \left[\int_0^{0.035} \bar{z} C_{evk}(t) \dot{t}(\bar{z},\tau_k) \mathrm{d}\bar{z} - 0.035 q_{ev}(\tau_k) \right]^2 (\tau_{k+1} - \tau) . \quad (49)$$

the inverse problem for the heat capacity $C_{evk}(t,\tau_k)$ at each k-th interval is reduced to finding the minimum of the functional by the method of conjugate gradients.

The solution of the HP' evaporator thermal conductivity inverse problem (32), (37) and (46) and the solution of the integral Equation (44) for determining the evaporator heat capacity was carried out using the developed program in Fortran [3] [4] [5].

In the conjugate gradient method, one-dimensional minimization in the permissible direction was carried out using the interpolation-extrapolation method [35]. The described algorithm for determining the piecewise function $C_{evk}(\delta t)$ with a known thermal resistance function $R_{HP}(t)$ was previously tested on several classical models of the inverse problems in thermal conductivity. The obtained results of these problems solving show that the heat capacity function $C_{evk}(\delta t)$ can be restored in all cases with an error of less than 5%. **Table 2** shows the results of solving the inverse problem of thermal conductivity for two cylindrical samples, a measuring sample with conductive heat transfer and a model sample with a local phase transition, with the same sample length of 3×10^{-3} m. The heat capacity is $C_0 = 1 \times 106$ J/m^3·K, thermal resistance $R_{sample} = 0.25 \times 10^2$ K/W, the heat of evaporation $Q_{vp} = 345$ kJ/kg ($C_4H_{10}O$) at the evaporator temperature $T_{ev} = 328.75$K (55.6˚C) and pressure $\bar{P} \sim 6.13 \times 10^5$ Pa , $Q_{ev} = 210$ W, heating velocity 3×10^{-3} K/s.

For a measuring sample with conductive heat transfer, all details are from Equation (22). For a model sample, the boundary conditions are given below in Equations (50) and (51):

$$\bar{z} = L_{ev} : \lambda \frac{\partial T}{\partial \bar{z}} = Q_{cond} . \quad (50)$$

Table 2. Calculated values of the relative heat capacity when heating two samples with different heat transfer parameters and the influence assessment of the various mathematical processing.

sample type	$\Phi(\xi)$	C/C_0
measuring sample with heat transfer by the thermal conductivity	$\Phi(\xi) = \xi$,	3.3
	$\Phi(\xi) = \exp(\xi)$,	3.3
model sample with heat transfer by the liquid evaporating and vapour condensing	$\Phi(\xi) = \xi$,	9.5
	$\Phi(\xi) = \exp(\xi)$,	11.8

$$\overline{z} = 0 : \lambda \frac{\partial T}{\partial \overline{z}} = Q_{ev} - G_{ev} \cdot Q_{vp} . \quad (51)$$

where the evaporation rate and the saturated vapor pressure are estimated as follows:

$$G_{ev} = const \frac{P_{vp} - \overline{P}}{\sqrt{2\pi RT/M}}; \; P_{vp} = \overline{P} \exp\left(-\frac{Q_{vp}}{RT}\right)$$

To calculate the heat capacity of the evaporator, a rather complex program was developed in FORTRAN, using computational equations based on the Simpson method [37] [38] [39] and Equation (37), which represents the most complete numerical iterative Crank-Nicholson scheme [37] [38] and for brevity is shown in **Figure 7**. All calculation details are given in [29] [30] [31], the iterative process is completed when the result $\delta C_{ev}/C_{ev}$ is obtained, which does not exceed the random error of the temperature growth rate and thermal power data:

$$\frac{\delta C_{ev}}{C_{ev}} = \sqrt{\left(\frac{\delta \dot{t}}{\dot{t}}\right)^2 + \left(\frac{\delta q_{ev}}{q_{ev}}\right)^2} \le 0.3 \text{ J/K} . \quad (52)$$

The results of the calculated solution of equation (44) in the range of temperature load on the HP's evaporator $\delta t = T_{ev} - T_B = (-5 \ldots +25)$ K are shown in **Figure 8**, the random error in calculating the heat capacity of the diethyl ether saturated evaporator does not exceed (2 - 3)%. The analysis of the calculated results C_{ev}/C_{ev0} of the capillary-porous evaporator heat capacity heated linearly in time can be carried out using the previously obtained equation for calculating the enthalpy (11), which takes into account all the details of heating and evaporation of diethyl ether.

The evaporation enthalpy of the working evaporator with boiling diethyl ether was estimated earlier in Equation (11), therefore we can substitute the known table values for diethyl ether [25] [26] [27] and can get an expression for the effective heat capacity of a linearly heated capillary-porous HP's evaporator at the ether boiling beginning:

$$C_{ev} = \frac{H_{ev}}{\dot{t}} = \frac{\left(345\ \text{kJ/kg} + 1.75\ \text{kJ/kg}\cdot\text{K} \times 11\ \text{K} + 2.34\ \text{kJ/kg}\cdot\text{K} \times 16\ \text{K}\right) \times 1.57 \times 10^{-4}\ \text{kg/s}}{3 \times 10^{-3}\ \text{K/s}} = 21.02\ \text{kJ/K}. \quad (53)$$

The ratio of the heat capacity of the evaporator with diethyl ether to the dry evaporator C_{ev}/C_{ev0} taking into account the heat capacity of the resistive heater C_{H2} = 1.2 kJ/K at the diethyl ether boiling beginning is as follows:

$$\frac{C_{ev}}{C_{ev0}} = \frac{C_{ev0} + H_{ev}/\dot{t}}{C_{ev0}} = 1 + \frac{H_{ev}/\dot{t}}{C_{ev0}} = \frac{21.02 + 1.2}{1.2} = 18.5. \quad (54)$$

which is very close to the maximum numerical value of the heat capacity of the HP's evaporator.

Equations (53) and (54) confirm the correspondence of the experimental and calculated thermophysical characteristics of diethyl ether located in the evaporator at a high temperature load.

4. Conclusions

1) The measurements of the surface temperature of short linear HP's with linear heating of the evaporator in time make it possible to unambiguously record an uneven drop in surface temperature. The HP's surface temperature values around the evaporator, which are close to constant, allow us to estimate a small drop in the transmitted thermal power in the HP's vapour channel. The constancy of the surface temperature around the evaporator also allows us to apply the method of solving the inverse problem of thermal conductivity (IPTC), and numerically obtain the extreme value of the heat capacity of the area (fragment) of the HP's evaporator. This calculated result was obtained for the first time.

2) The HP's external surface temperature of the capillary-porous evaporator, which is close to a constant value with monotonous heating, confirms the boiling process beginning and allows us to estimate the complex thermophysical parameters of diethyl ether in the evaporator.

3) With step-by-step regularization of the inverse problem solution of the HP's thermal conductivity and piecewise smooth polynomial approximation of unknown coefficients, it is possible to minimize the error in restoring the evaporator heat capacity using a polynomial-exponential approximation function that restricts the range of acceptable heat capacity values by only positive values.

Acknowledgements

The author expresses gratitude to Tsvetkov Oleg Borisovich, Professor of ITMO, St. Petersburg, for his active participation in the discussion of this article at the Institute's conferences. The author expresses special gratitude to the management of "RUDETRANSSERVICE", Veliky Novgorod, for providing instruments and equipment for conducting experimental determination of thermal characteristics of heat pipes with heating close to linear in time.

Conflicts of Interest

The author declares no conflicts of interest regarding the publication of this paper.

References

[1] Brebbia, C.A. and Dominguez, J. (1998) Boundary Elements: An Introductory Course. WIT Press & Computational Mechanics Publication, Boston & Southampton, 325 p.

[2] Nakayama, A. and Kuwanara, F. (2008) A General Bioheat Transfer Model Based on the Theory of Porous Media. *International Journal of Heat and Mass Transfer*, **51**, 3190-3199. https://doi.org/10.1016/j.ijheatmasstransfer.2007.05.030

[3] Beck, J., Blackwell, B. and Clair, C. (1985) Inverse Heat Conduction Ill Posed Problems. Wiley & Sons, New York, 308 p.

[4] Carslaw, H.S. and Jaeger, J.C. (1986) Conduction of Heat in Solids. Oxford University Press, Oxford, 510 p.

[5] Lykov, A.V. (1967) Theory of Thermal Conductivity. Higher School, Moscow, 600 p.

[6] Platunov, E. (1973) Thermophysical Measurements in a Monotonic Mode. Energy, Moscow, 144 p. (In Russian)

[7] Isachenko, V.P., Osipova, V.A. and Sukomel, A.S. (1981) Heat Transfer. Energoizdat, Moscow, 416 p. (In Russian)

[8] Kutateladze, S.S. (1979) Fundamentals of the Heat Transfer Theory. 5th Edition, Atomizdat, Moscow, 416 p. (In Russian)

[9] Denisov, A.M. (1994) Introduction to the Theory of Inverse Problems. MU, Moscow, 208 p. (In Russian)

[10] Tikhonov, A.M. (1963) On the Solution of Incorrectly Set Tasks and the Method of Regularization. *DAN USSR*, **151**, 501-504.

[11] Tikhonov, A.N. and Arsenin, V.Ya. (1979) Methods for Solving Incorrect Problems. Science, Moscow, 284 p. (In Russian)

[12] He, J.-H. (1999) Variational Iteration Method—A Kind of Non-Linear Analytical Technique: Some Examples. *International Journal of Non-Linear Mechanics*, **34**, 699-708. https://doi.org/10.1016/S0020-7462(98)00048-1

[13] He, J.-H. (2006) Some Asymptotic Methods for Strongly Nonlinear Equations. *International Journal of Modern Physics B*, **20**, 1141-1199. https://doi.org/10.1142/S0217979206033796

[14] Lu, J. (2007) Variational Iteration Method for Solving Two-Point Boundary Value Problems. *Journal of Computational and Applied Mathematics*, **207**, 92-95. https://doi.org/10.1016/j.cam.2006.07.014

[15] Yan, L., Fu, C.-L. and Yang, F.L. (2008) The Method of Fundamental Solutions for the Inverse Heat Source Problem. *Engineering Analysis with Boundary Elements*, **32**, 216-222. https://doi.org/10.1016/j.enganabound.2007.08.002

[16] Seryakov, A.V. (2018) Intensification of Heat Transfer Processes in the Low Temperature Short Heat Pipes with Laval Nozzle Formed Vapour Channel. *American Journal of Modern Physics*, **7**, 48-61. https://doi.org/10.11648/j.ajmp.20180701.16

[17] Seryakov, A.V., Shakshin, S.L. and Alekseev, P. (2017) The Droplets Condensate Centering in the Vapour Channel of Short Low Temperature Heat Pipes at High Heat Loads. *Journal of Physics: Conference Series*, **891**, Article ID: 012123. https://doi.org/10.1088/1742-6596/891/1/012123

[18] Seryakov, A.V. (2019) Computer Modeling of the Vapour Vortex Orientation Changes in the Short Low Temperature Heat Pipes. *International Journal of Heat and Mass Transfer*, **140**, 243-259. https://doi.org/10.1016/j.ijheatmasstransfer.2019.04.123

[19] Seryakov, A.V. (2016) Characteristics of Low Temperature Short Heat Pipes with a Nozzle-Shaped Vapour Channel. *Journal of Applied Mechanics and Technical Physics*, **57**, 69-81. https://doi.org/10.1134/S0021894416010089

[20] Seryakov, A.V. (2017) The Study of Condensation Processes in the Low-Temperature Short Heat Pipes with a Nozzle-Shaped Vapour Channel. *Engineering*, **9**, 190-240. https://doi.org/10.4236/eng.2017.92010

[21] Seryakov, A.V. (2019) Numerical Modeling of the Vapour Vortex. *Journal of High Energy Physics, Gravitation and Cosmology*, **5**, 218-234. https://doi.org/10.4236/jhepgc.2019.51013

[22] Fowler, R.H. (1936) Statistical Mechanics. 2nd Edition, Cambridge University Press, London.

[23] Chapman, S. and Cowling, T.G. (1953) The Mathematical Theory of Non-Uniform Gases. Cambridge University Press, London, 447 p.

[24] CFdesign 10.0 2009. Version 10.0-20090623. User's Guide.

[25] Mackay, D., Shiu, W., Ma, K. and Lee, S. (2006) Handbook of Physical-Chemical Properties and Environmental Fate for Organic Chemicals. Vol. III. Oxygen Containing Compounds. Taylor and Francis, Abingdon-on-Thames.

[26] (1976) Tables of Physical Values. Guide under the ed. of Kikoin I.K. Atomizdat, Moscow. 1008 p.

[27] Vargaftic, N.B. (1972) Handbook of Thermophysical Properties of Gases and Liquids. Publishing House of Physics and Mathematical Literature, Moscow, 721 p.

[28] Faghri, A. (1995) Heat Pipe Science and Technology. Taylor and Francis, Washington DC.

[29] Seryakov, A.V. and Alekseev, A.P. (2020) A Study of the Short Heat Pipes by the Monotonic Heating Method. *Journal of Physics*: *Conference Series*, **1683**, Article ID: 022051. https://doi.org/10.1088/1742-6596/1683/2/022051

[30] Seryakov, A.V. and Alekseev, A.P. (2020) Investigation of Short Heat Pipes by the Method of Monotonous Heating. *III International Conference* "*Modern Problems of Thermophysics and Energy*", Moscow, 19-23 October 2020, 270-272.

[31] Seryakov, A.V. and Alekseev, A.P. (2020) Investigation of Short Linear Heat Pipes by Solving the Inverse Problem of Thermal Conductivity. *Reshetnev Readings. Materials of the XXIV International Scientific and Practical Conference Dedicated to the Memory of the General Designer of Rocket and Space Systems*, Krasnoyarsk, 10-13 November 2020, Part 1, 144-146.

[32] Odibat, Z.M. and Momani, S. (2006) Application of Variational Iteration Method to Nonlinear Differential Equations of Fractional Order. *International Journal of Nonlinear Sciences and Numerical Simulation*, **7**, 27-34. https://doi.org/10.1515/IJNSNS.2006.7.1.27

[33] Farcas, A. and Lesnic, D. (2006) The Boundary-Element Method for the Determination of a Heat Source Dependent on One Variable. *Journal of Engineering Mathematics*, **54**, 375-388. https://doi.org/10.1007/s10665-005-9023-0

[34] Elsholts, L.E. (2008) Calculus of Variations: A Textbook for Physical and Physical-Mathematical Faculties of Universities. Moscow Publishing House, Moscow, 205 p. (In Russian)

[35] Elsholts, L.E. (1969) Differential Equations and Calculus of Variations. Nauka, Moscow. (In Russian)

[36] Tslaf, L.Y. (2005) Calculus of Variations and Integral Equations: A Reference Guide. 3rd Edition, St. Petersburg Publishing House, St. Petersburg, 192 p. (In Russian)

[37] Marchuk, G.I. (1980) Methods of Computational Mathematics. Nauka, Moscow, 536 p. (In Russian)

[38] Tikhonov, A.N. and Samarsky, A.A. (1966) Equations of Mathematical Physics. Nauka, Moscow, 724 p. (In Russian)

[39] Kalitkin, N.N. (1978) Numerical Methods. Nauka, Moscow, 512 p. (In Russian)

Nomenclature

$a = \lambda / C_p \cdot R_{HP}$—coefficient of HP's thermal diffusivity;
a^k = k-th calculated component of the thermal diffusivity coefficient, m^2/s;
C_{eff}: effective heat capacity of the HP, J/K;
$C_{HP}(t)$—HP's heat capacity as a whole, J/K;
$c_v(t)$—HP's volume heat capacity, $J/m^3 \cdot K$;
$c_v(T)$—HP's specific isochoric heat capacity, J/kg·K;
C_{ev0}—heat capacity of the dry evaporator, J/K;
C_{ev}—heat capacity of the evaporator with diethyl ether, J/K;
C_{ev}—calculated heat capacity of the evaporator, J/K;
C_f—diethyl ether heat capacity, J/kg·K;
C_{vp}—heat capacity of diethyl ether moist vapour, J/kg·K;
C_{fev}—heat capacity of diethyl ether on the evaporator surface, J/kg·K;
E_{H2}—thermal power of the resistive heater, W;
$F_{HP}(sz)$—HP's cross-sectional area, m^2;
G_f—mass flow rate of diethyl ether liquid phase in the evaporator, kg/s;
G_{mix}—mass flow of the moist saturated vapour over the evaporator, kg/s;
G_{vp}—mass flow rate of dry saturated vapour over the evaporator, kg/s;
$(1 - x_{ev}) = G'/(G' + G)$ —the degree of moisture vapour in the evaporator;
g_k—the derivative of the heat capacity components;
H_{ev}—enthalpy of the HP's evaporator, W;
L_{HP}—HP's length, m;
L_{ev}—the thickness of the capillary porous evaporator, m;
$\overline{P}$ —the average pressure in the vapour channel, Pa;
P_{ev}—pressure above the evaporator, Pa;
P_{fcond}—pressure on the condensation surface, Pa;
P_v—the vapour pressure inside the toroidal vortex, close to the condensation pressure P_{fcond};
Pr—the Prandtl number of the diethyl ether vapour;
Q_{ev}—heat input to the evaporator, W;
Q_{cond}—heat of condensation, W;
R_c—thermal resistance of the lubricant layer, K/W;
R_{ev}—thermal resistance of the evaporator, K/W;
R_w—thermal resistance of the metal cover, K/W;
$R_{HP}(T)$—HP's thermal resistance, K/W;
$r(T_B)$ —specific heat of evaporation of diethyl ether, kJ/kg;
T_B—boiling point of the diethyl ether, K;
T_{cal}—the temperature of the flowing water in the vortex calorimeter;
T_{cond}—condensation surface temperature T, K;
$\overline{T}_{fcond}$ —the average temperature of the diethyl ether film on the HP's condensation surface, K;
$\overline{T}_{fev}$ —the average temperature of diethyl ether boiling microlayer on the HP's lower cover surface, K;

$T_{HP}(\bar{z})$ —the temperature inside the HP's vapour channel at a height of $\bar{z}$ above the evaporator, K;

T_{ev}—stationary temperature of the grid evaporator saturated with the diethyl ether, K;

T_{sc}—stationary temperature of the evaporator metal mesh, K;

T_v—he vapour temperature inside the toroidal vapour vortex, K;

$\dot{t}$ —temperature growth rate, K/s;

$\boldsymbol{v}$—vapour (and liquid) phases flow velocity inside the capillary-porous evaporator, m/s;

x_{ev}—the degree of vapour moisture in the evaporator;

Y—parameter of the additional source function, J;

$\bar{z} = z/L_{HP}$ —dimensionless longitudinal coordinate;

u_v, v_v—axial and tangential components of the vortex velocity in the HP's vapour channel, m/s;

Greek

α_{cal}—heat transfer coefficient in the vortex flow calorimeter, W/m^2·K;

α_{cond}—heat transfer coefficient in the HP's condensation region, W/m^2·K;

δ_{fcond}—the average thickness of the diethyl ether film on the condensation surface, m;

δ_w—the thickness of the flat metal bottom cover, m;

η—Lagrange multiplier;

λ_{eff}—effective thermal conductivity, W/m·K;

$\bar{\lambda}_{HP}$ —effective thermal conductivity of the HP, W/m·K;

λ_f—thermal conductivity of diethyl ether, W/m·K;

$\lambda(t)$—HP thermal conductivity coefficient, W/m·K;

λ_{sc}—thermal conductivity coefficient of metal mesh evaporator frame, W/m·K;

λ_w—thermal conductivity coefficient of metal top and bottom covers, W/m·K;

μ_f—friction coefficients;

ξ—condensation coefficient defined as the ratio of the number of vapour molecules condensing over the total number of molecules which strikes the surface;

Π—the porosity of the evaporator and insert (wick) in the HP's vapour channel;

ρ_{HP}—HP's density, kg/m^3;

ρ_{vp}^{mix} —the density of moist vapour inside the vapour channel, kg/m^3;

ρ_v—the vapour density inside the toroidal vortex, kg/m^3;

$\bar{\rho}_{ev}$, kg/m^3—average evaporator density, kg/m^3;

τ—time, s;

$\Delta\tau_k$—time step for calculations and measurements, s;

Φ_{df}—dissipative functions;

χ—Lagrange multiplier;

ψ—the mass fractions of the HP's components;